# Characterizing Aqueous Solution Conformations of a Peptide Backbone Using Raman Optical Activity Computations

Parag Mukhopadhyay, Gérard Zuber, and David N. Beratan
Departments of Chemistry and Biochemistry, Duke University, Durham, North Carolina 27708

ABSTRACT Mounting spectroscopic evidence indicates that alanine predominantly adopts extended polyproline II (PPII) conformations in short polypeptides. Here we analyze Raman optical activity (ROA) spectra of *N*-acetylalanine-*N*′-methylamide (Ala dipeptide) in $H_2O$ and $D_2O$ using density functional theory on Monte Carlo (MC) sampled geometries to examine the propensity of Ala dipeptide to adopt compact right-handed ($\alpha_R$) and left-handed ($\alpha_L$) helical conformations. The computed ROA spectra based on MC-sampled $\alpha_R$ and PPII peptide conformations contain all the key spectral features found in the measured spectra. However, there is no significant similarity between the measured and computed ROA spectra based on the $\alpha_L$- and $\beta$-conformations sampled by the MC methods. This analysis suggests that Ala dipeptide populates the $\alpha_R$ and PPII conformations but no substantial population of $\alpha_L$- or $\beta$-structures, despite sampling $\alpha_L$- and $\beta$-structures in our MC simulations. Thus, ROA spectra combined with the theoretical analysis allow us to determine the dominant populated structures. Including explicit solute-solvent interactions in the theoretical analysis is essential for the success of this approach.

## INTRODUCTION

Conformational analysis of alanine-containing polypeptides suggests that the polyproline II (PPII) is the major backbone conformation in aqueous solution. For example, Kallenbach and co-workers recently showed that alanine-containing peptides possess over 90% extended conformations (i.e., PPII and $\beta$-structures) (1). The authors, however, did not rule out the possibility of the presence of compact ($\alpha_R$, $\alpha_L$) conformations of alanine in aqueous solution and suggested that such compact structures are present, albeit not dominant. Here, we use Raman optical activity (ROA) to examine the propensity of Ala dipeptide, which contains a peptide backbone with a single alanine, to adopt compact structures like the right-handed ($\alpha_R$) and left-handed ($\alpha_L$) helical conformations in aqueous solution. We find that Ala dipeptide adopts both the extended PPII and compact $\alpha_R$-conformations, which are the dominant conformations in aqueous solution.

Experimental and theoretical studies of polypeptides (2) suggest that short polypeptides can adopt secondary structures in aqueous solution. For example, the hepta-alanine polypeptide Ac-$X_2A_7O_2$-$NH_2$ (XAO; X and O denote diaminobutyric acid and ornithine, respectively) in aqueous solution was suggested to be an ensemble of $\beta$-turn, $\beta$-strand, and PPII conformations (3–5). A combination of Fourier transform infrared, vibrational circular dichroism, electronic circular dichroism, Raman, and NMR spectroscopic studies probed shorter alanine-based cationic peptides (e.g., trialanine, tetraalanine, and H-AAKA-OH). These studies indicated that these shorter peptides have a higher fraction of PPII than $\beta$-strand or $\alpha_R$-conformations (6). ROA studies of a series of $A_2$-$A_5$ peptides suggest that the PPII population increases with the number of alanines (7). Taken together, these results provide compelling evidence that alanine-containing peptides in water populates PPII conformations. Molecular dynamics (MD) simulations of alanine-containing peptides in water indicate the sampling of $\alpha_R$-motifs, in addition to the PPII and $\beta$-conformations (8).

Graf's combined MD and NMR studies, however, show that there is no detectable population of the $\alpha_R$-conformation in aqueous solutions of $A_3$-$A_7$ peptides and that these short polyalanine peptides in water populate the PPII conformation almost exclusively (9). Following Graf's conformational analysis of $A_3$-$A_7$ peptides, Hummer and co-workers studied polyalanine peptide ($A_5$) conformations in aqueous solution using MD simulations to address the question of whether the commonly used force fields overpopulate the $\alpha$-helical conformations of polyalanine peptides (10). They concluded that the NMR data are consistent with force fields that give a small $\alpha$-helical population of polyalanine peptide and do not require exclusive formation of the PPII structure. Our combined Monte Carlo (MC) and ROA studies of Ala dipeptide show that the shortest alanine-containing peptide exists as a mixture of PPII and $\alpha_R$-conformations in aqueous solution.

Chiroptical properties are sensitive to molecular geometry and to solvation (11–13). ROA is a chiroptical spectroscopy that measures the difference in the intensity of Raman scattered right- and left-circularly polarized light and is utilized to characterize aqueous solution conformations of the peptide backbone in polypeptides and proteins (14,15). ROA studies of polypeptides suggest that water promotes structural fluctuations between $\alpha_R$-, PPII, and $\beta$-conformations (16). The ROA spectrum is the superposition of spectra arising from all conformations of polypeptides in solution (14), and thus,

*Submitted May 16, 2008, and accepted for publication August 26, 2008.*

Address reprint requests to David N. Beratan, Dept. of Chemistry, Box 90346, Duke University, Durham, NC 27708. Fax: 919-660-1605; E-mail: david.beratan@duke.edu.

Editor: Gregory A. Voth.


0006-3495/08/12/5574/13 $2.00

doi: 10.1529/biophysj.108.137596

ROA analysis can be used to characterize solution conformations of peptide units in polypeptides.

The theoretical framework for ROA is well known (17–19). Accurate time-dependent density functional theory (TD-DFT) calculations of ROA are accessible using the resolution of identity approximation (RI-J) (20–22) and the Becke-Lee-Yang-Parr (BLYP) functional with the depolarized right-angle scattering (rDPS) basis set (23). ROA spectra are predicted to be very sensitive to both molecular conformation (24–28) and solvation, which were studied previously using continuum solvent models (29). Herrmann et al. (30) and Pecul et al. (29) analyzed ROA spectra of polypeptides using a single conformation in the gas phase and in an implicit solvent, respectively. Since ROA studies of polypeptides indicate that water facilitates conformational fluctuations (16), modeling polypeptide conformations in explicit solvent, and subsequently utilizing modeled structures to compute ROA spectra, may improve the effectiveness of ROA simulations for polypeptides.

Despite extensive experimental and theoretical study, there is no consensus on Ala dipeptide's structure in aqueous solution. NMR studies are consistent with both 1), an equal population of PPII and $\alpha_R$-conformations (31,32), and 2), a dominant PPII conformation (33,34). The later composition is supported by two-dimensional (2D) infrared (IR) spectroscopy (35). However, Raman spectroscopy suggests that $C7_{eq}$, PPII, and $\alpha_R$-conformations all exist in aqueous solution (36). MC and MD simulations of Ala dipeptide indicate either 1), PPII (8,37,38) or $\alpha_R$-structures dominate (39–42), or 2), a comparable population of PPII and $\alpha_R$-structures dominates (43–45), depending on the force field used. Thus, a debate remains as to whether PPII is the dominant conformation of Ala dipeptide in aqueous solution. The significant variation in the description of Ala dipeptide conformations warrants further analysis and suggests the utility of linking chiroptical simulations with experimental studies. Our ROA simulations combined with experimental data show that Ala dipeptide populates both the $\alpha_R$ and PPII conformations in aqueous solution; and hence, it is erroneous to ascribe all experimental signal to one dominant conformation, namely the PPII.

We present TD-DFT calculations of backscattered circular polarization (SCP) ROA based on MC simulation of Ala dipeptide in aqueous solution. Simulated Raman and ROA spectra constructed using the collection of $H_2O$-Ala clusters (see Methods for more details) with $\alpha_R$ and PPII conformations of Ala dipeptide are consistent with experiments. However, there is no significant similarity between the measured and computed Raman or ROA spectra for the set of $H_2O$-Ala clusters with $\alpha_L$- and $\beta$-conformations of Ala dipeptide. Thus, these calculations facilitate assignment of the observed ROA spectral features to corresponding secondary structures that characterize the populated conformations of the peptide in aqueous solution. The interpretation of the experimental data enabled by the calculations helps in understanding the relationship between peptide conformations and ROA spectra. Our calculations also provide substantial predictive value. For example, our calculations demonstrate that ROA can distinguish between left- and right-handed helical conformations of peptides in aqueous solution; and hence, ROA can be used to differentiate the chirality associated with the handedness of helical conformations of peptides.

Previous ROA analysis using four Ala dipeptide conformations ($\beta$, $\alpha_R$, $\alpha_L$, PPII), each hydrogen bonded to four water molecules and embedded in an implicit solvent model, showed that the computed spectra of the PPII structure best explained the experimental ROA spectrum (46). It was also suggested that $\alpha_R$, $\alpha_L$, and ''other conformations'' of Ala dipeptide may be present in aqueous solution (46). Those ROA calculations were performed using restricted Hartree-Fock theory with a split valence plus basis set and neglected the effects of explicit water on the chiroptical response tensor (46). Pecul et al. showed recently that solvent influences on the chiroptical response tensor should be included when computing solvent effects on ROA (29). Jalkanen et al. recently computed the ROA spectra of a single $(H_2O)_4$-Ala dipeptide cluster, with the PPII conformation of the dipeptide, embedded in implicit solvent models using the B3PW91/B3LYP exchange correlation functionals with the aug-cc-pVDZ basis set (47). Those simulated ROA spectra (46–48) were in qualitative agreement with the experimental spectra, which provided the impetus for computing the ROA spectrum with improved accuracy for aqueous Ala dipeptide solutions using geometry sampling as an explicit part of the calculation. We now show that including explicit solute-solvent interactions is essential for computing the ROA of Ala dipeptide accurately in water and that TD-DFT computation (with the RI-J approximation and rDPS basis set) using MC-sampled geometries in aqueous solution provides a suitable means to analyze the ROA spectra of polypeptides and determine the dominant populated conformations of polypeptides in solution.

## METHODS

Two sets of MC computer simulations of Ala dipeptide in $H_2O$ were performed using the optimized potential for liquid simulations-all atom (OPLS-AA) force field (49) and TIP4P water model (50). First, low-energy conformations of Ala dipeptide in $H_2O$ were identified that characterize potentially populated regions of the Ramachandran map using MC free-energy simulations. Second, $H_2O$ configurations were sampled with fixed backbone dihedral angles ($\phi$ and $\psi$; Fig. 1 *A*) for the dipeptide. The fixed peptide geometries were selected from low-energy regions of the Ramachandran map (Fig 1*B*). $H_2O$-Ala dipeptide cluster structures from the second set of MC simulations (sampling water configuration with fixed-peptide geometry) were optimized using DFT. Each $H_2O$-Ala dipeptide cluster has 10 water molecules within a cutoff distance of 0.5 nm from the hydrogen-bond donor (NH) and acceptor (O, N) atoms of Ala dipeptide (Fig. 1 *A*). Following geometry optimization of the $H_2O$-Ala dipeptide cluster, the structures were used to compute the backscattering ROA and Raman spectra using TD-DFT with the RI-J approximation, the BLYP functional, and the rDPS basis set.

### MC simulations

Free energy perturbation theory (51) was used to calculate the potential of mean force (PMF) that describes the relative free energy difference between

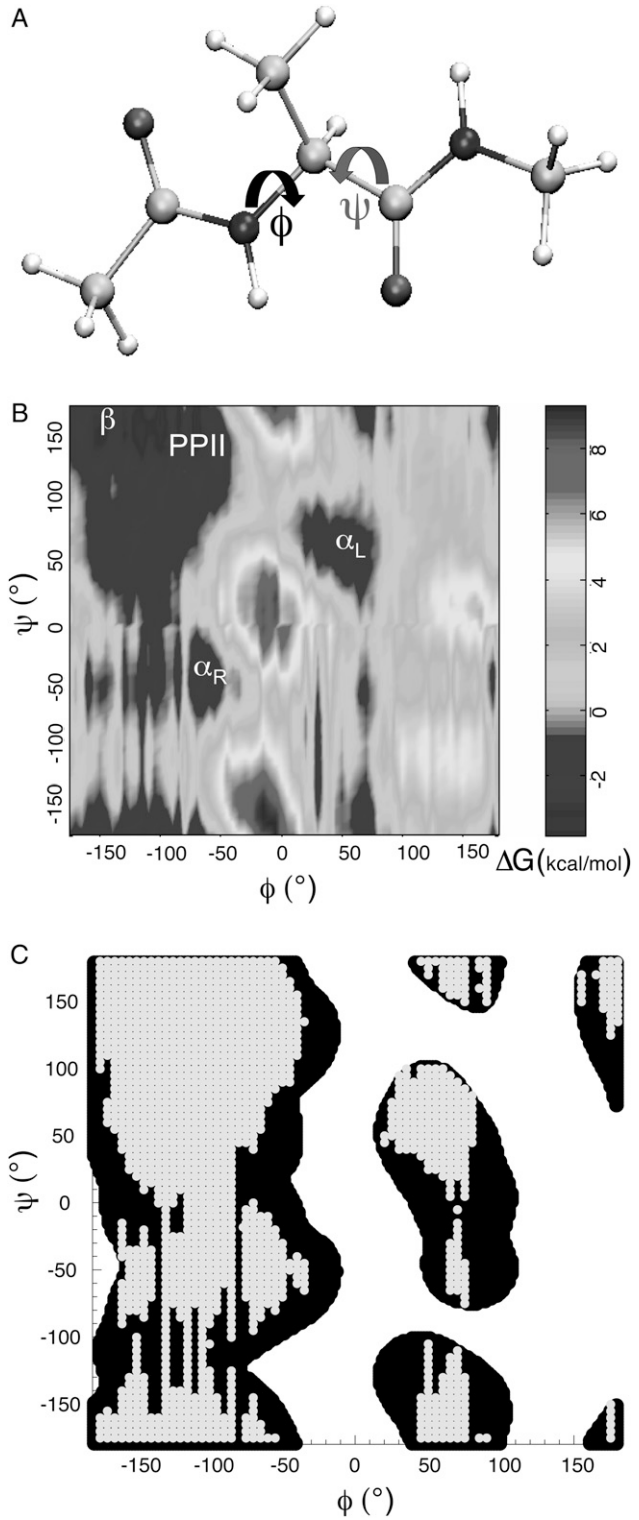


FIGURE 1 (*A*) Ball and stick model for the *N*-acetylalanine-*N′*-methylamide (Ala dipeptide). The peptide backbone structure in Ala dipeptide is defined by $\phi$- and $\psi$-dihedral angles. (*B*) Free energy differences of Ala dipeptide conformations in water computed using MC simulations. $\alpha_R$, $\alpha_L$, $\beta$, and PPII conformational regions are shown on the Ramachandran map. (*C*) the computed $\phi$- and $\psi$-distribution (*gray*) resembles the empirically derived $\phi$, $\psi$ distribution of amino acid residues (*black*) in neither canonical helix nor sheet secondary structures in protein x-ray crystal structures (61).

Ala dipeptide conformations as a function of the peptide backbone dihedral angles. One-dimensional PMFs were calculated first with $\phi$ fixed and $\psi$ varied from 0° to 360° in 5° increments. Then $\psi$ was fixed and $\phi$ was varied from 0° to 360° in 5° increments. A 2D plot of the free energy difference for $\phi = 80°$, $\psi = 80°$, the reference conformation, and all $\phi$, $\psi$ pairs were calculated from the one-dimensional PMFs. The resulting 2D plots identify low-energy conformations of Ala dipeptide in water.

MC simulations of Ala dipeptide in a box of 500 water molecules were performed using BOSS (51) at 25°C and 1 atm (NPT ensemble) with periodic boundary conditions. Long-range electrostatic interactions were evaluated by the Ewald method (52). The OPLS-AA force field, TIP4P water, and AM1 (53) based CM1A (54) partial atomic charges for the solute and solvent were used in the MC simulations. A more detailed description of the MC move and the atomic charge-partitioning scheme appears in Jorgensen and Tirado-Rives. (51).

## DFT calculations of ROA

Zuber et al. recently demonstrated accurate and efficient prediction of ROA spectra using TD-DFT (22). The approach avoids calculating the four-center Coulomb integrals and omits contributions of the electric dipole-electric quadrupole polarizability tensor to the ROA differential scattering cross section. Luber et al. also showed recently that the contribution of the electric dipole-electric quadrupole polarizability tensor to the ROA intensities can be neglected for the amide I, amide II, and amide III vibrational modes for peptides (below 2000 $cm^{-1}$) (55). We use the same scheme in the off-resonance approximation (56) to calculate the circular difference differential scattering cross sections per unit solid angle $(-\Delta^n d\sigma(\pi)_{SCP}/d\Omega)$ for (57) SCP with naturally polarized ($n$) incident light:

$$\frac{-\Delta^n d\sigma(\pi)_{SCP}}{d\Omega} \approx \frac{K}{c}(48\beta_G^2), \tag{1}$$

where $c$ is the speed of light, $\beta_G^2$ is the anisotropic ROA invariant, and $K$ is

$$K = \frac{10^7}{9}\pi^2\mu_o^2 c^4 \tilde{\nu}_o \left(\frac{\omega_o}{200\pi c} - \Delta\tilde{\nu}_p\right)^3, \tag{2}$$

where $\omega_o = 2\pi\nu_o$ is the frequency of the incident light, $\Delta\tilde{\nu}_p$ is the Raman frequency shift (in $cm^{-1}$), $c$ is the speed of light (in $ms^{-1}$), and $\mu_o$ is the permittivity of vacuum.

Placzek polarizability theory writes (58)

$$\beta_G^2 = \frac{1}{2}\sum_{\mu\nu}(3\alpha_{\mu\nu}G'_{\mu\nu} - \alpha_{\mu\mu}G'_{\nu\nu}), \tag{3}$$

where $\alpha_{\mu\nu}G'_{\mu\nu}$ is

$$\alpha_{\mu\nu}G'_{\mu\nu} = \frac{h}{8\pi^2 c\Delta\tilde{\nu}_p}\sum_{\alpha,\beta}\sum_{i,j}\left(\frac{\partial\alpha^e_{\mu\nu}}{\partial x_i^\alpha}\right)_0\left(\frac{\partial G'^e_{\mu\nu}}{\partial x_j^\beta}\right)_0 L^x_{\alpha i,p}L^x_{\beta j,p}, \tag{4}$$

where $L^x_{\alpha i,p}$ is the $i$th component of the Cartesian displacement vector of nucleus $\alpha$ for normal mode $p$, and $\alpha^e_{\mu\nu}$ and $G'^e_{\mu\nu}$ are the elements of the electric dipole-electric dipole polarizability tensor and the imaginary part of the electric dipole-magnetic dipole polarizability tensor, respectively. The index 0 indicates that the derivatives of the electronic tensors are computed at the equilibrium nuclear geometry.

The geometries of $H_2O$-Ala dipeptide clusters from the second set of MC simulations were optimized using DFT implemented in TURBOMOLE (version 5.6) (59) with the BLYP correlation-exchange functional and the SVP basis set. The normal coordinates of the $H_2O$-Ala dipeptide clusters were computed from the molecular Hessian, which was determined for the optimized geometry. Optimizations of some of the $H_2O$-Ala dipeptide cluster structures lead to imaginary frequencies; and hence, such structures were not included in the ROA calculations. A 532 nm incident laser wavelength was used for tensor calculations, which were performed using TD-DFT with the

BLYP functional, the rDPS basis set, and the [7s3p3d1f]/[3s2p1d] auxiliary basis set (60). All the calculations were performed in a gauge-independent dipole-velocity formulation using the RI-J. The Cartesian gradients of the polarizability tensors were evaluated numerically using the $6N$-displaced geometries, where $N$ is the number of atoms. The $6N$ geometries were obtained from the optimized geometries of the $H_2O$-Ala dipeptide clusters using a displacement of $\pm 10^{-3}$ atomic units along the Cartesian coordinates.

The molecular Hessian of the optimized geometry of $H_2O$-Ala dipeptide clusters were used to compute the vibrational frequencies and normal coordinates of $D_2O$-Ala dipeptide structures. Thus, we used the $H_2O$-Ala dipeptide structures from the MC simulations to compute the ROA and Raman spectra of $D_2O$-Ala dipeptide clusters. The ROA and Raman spectra of the $D_2O$-Ala dipeptide clusters were then computed using Eq. 4.

The total Raman (${}^{n}d\sigma$) and ROA ($-\Delta^{n}d\sigma$) scattering cross sections of a Ala dipeptide-water cluster is the sum of scattering cross sections of the peptide (${}^{n}d\sigma_{p}, -\Delta^{n}d\sigma_{p}$), water (${}^{n}d\sigma_{W}, -\Delta^{n}d\sigma_{W}$), and peptide-water interactions (${}^{n}d\sigma_{pWI}, -\Delta^{n}d\sigma_{pWI}$). Hence, the total Raman and ROA scattering cross sections is

$$ {}^{n}d\sigma = {}^{n}d\sigma_{p} + {}^{n}d\sigma_{W} + {}^{n}d\sigma_{pWI} \quad (5) $$

$$ -\Delta^{n}d\sigma = -(\Delta^{n}d\sigma_{p} + \Delta^{n}d\sigma_{W} + \Delta^{n}d\sigma_{pWI}). \quad (6) $$

Thus, the relative contributions of the Raman and ROA scattering cross sections of the dipeptide, water, and peptide-water interactions can be compared to the total ROA and Raman scattering cross sections of the Ala dipeptide-water cluster.

## RESULTS

### Low-energy conformations of Ala dipeptide in water

Fig. 1 shows the difference in free energy ($\Delta G$) of Ala dipeptide conformations in water computed using MC simulations. The $\alpha_R$, $\alpha_L$, $\beta$, and PPII conformational regions are populated by the dipeptide (Fig. 1 *B*), in agreement with previous molecular mechanics force field simulations (38,43). Fig. 1 *C* shows that the computed distribution of $\phi$- and $\psi$-dihedral angles (for Ala dipeptide conformations with $\Delta G < 0$) also resembles the $\phi$, $\psi$ distribution of amino acid residues that are not found in either canonical helix or sheet secondary structures in protein x-ray crystal structures (61). Ala dipeptide explores both the right-handed ($\alpha_R$) and left-handed ($\alpha_L$) helical conformations, in agreement with previous MD and MC simulation studies (37,38,43). Thus, our MC simulations of aqueous Ala dipeptide indicate that the $\alpha$-helical conformations are stabilized by solvation.

### Structures of $H_2O$-Ala dipeptide clusters

$H_2O$-Ala dipeptide clusters from the MC simulations, corresponding to the low-energy regions ($\alpha_R$, $\alpha_L$, $\beta$, and PPII; Fig. 1 *B*) of the Ramachandran map, were optimized using quantum mechanical energy minimization (see Methods for details). The peptide backbone dihedral angles change upon geometry optimization. However, each peptide conformation, before and after geometry optimization, occupies the same region of the Ramachandran map (Supplementary Material, Fig. S1). Following geometry optimization of the $H_2O$-Ala dipeptide cluster, the structures were used for computing ROA and Raman spectra using TD-DFT (see Methods for details).

### ROA and Raman spectra of $H_2O$- and $D_2O$-Ala dipeptide clusters

Fig. 2 shows the computed ROA (*A* and *C*) and the Raman (*B* and *D*) spectra using $H_2O$-Ala dipeptide clusters. The computed spectra are averaged over 30 $H_2O$-Ala dipeptide structures with $\phi$- and $\psi$-dihedral angles from the PPII (*inset* in Fig. 2 *A*) and $\alpha_R$ (*inset* in Fig. 2 *C*) conformational regions of the Ramachandran map. The ROA spectra computed using both the PPII and $\alpha_R$-conformations contain spectral features found in the measured spectrum. For example, ROA bands (*a–f* in Fig. 2 *A*) at 395 $cm^{-1}$ (*a*), 940 $cm^{-1}$ (*b*), 1140 $cm^{-1}$ (*c*), 1560 $cm^{-1}$ (*e*, amide II), 1665 $cm^{-1}$ (*f*, amide I), and the couplet centered at ~1300 $cm^{-1}$ (*d*, extended amide III) are predicted in the computed spectrum using a set of Ala dipeptide conformations with $-80° \le \phi \le -60°$ and $130° \le \psi \le 150°$ (*inset* in Fig. 2 *A*), which is the set of structures from the PPII conformational region on the Ramachandran map. Thus, these ROA bands are attributed to the $H_2O$-Ala dipeptide structures with PPII conformations. The range of $\phi, \psi$ values ($-80° \le \phi \le -60°$ and $130° \le \psi \le 150°$) for the PPII conformations of Ala dipeptide in aqueous solution determined from our ROA analysis is consistent with the range of values ($-95° \le \phi \le -45°$ and $95° \le \psi \le 145°$) determined by 2D IR spectroscopy (35). Barron and coworkers have shown that positive ROA bands at ~1318 $cm^{-1}$ and ~1670 $cm^{-1}$ characterize PPII conformations of polypeptides (14,62), also consistent with our ROA analysis.

Fig. 2 *C* shows that the ROA bands (*a–f*) at 395 $cm^{-1}$ (*a*), 940 $cm^{-1}$ (*b*), 1140 $cm^{-1}$ (*c*), 1380 $cm^{-1}$ (*e*, C$\alpha$-H bend), 1450 $cm^{-1}$ (*f*), and the positive-negative couplet centered at ~1300 $cm^{-1}$ (*d*, extended amide III) are predicted in the computed spectrum using a set of Ala dipeptide conformations ($-50° \le \phi \le -100°$ and $-50° \le \psi \le 0°$) from the $\alpha_R$-region of the Ramachandran map (*inset* in Fig. 2 *C*). Thus, these ROA bands can be attributed to the $H_2O$-Ala dipeptide structures with $\alpha_R$-conformations of the dipeptide. Interestingly, the ROA spectrum computed using the set of $\alpha_R$-structures show a sequence of $-/-$ bands in the frequency range of 300–400 $cm^{-1}$ (Fig. 2 *C*), consistent with the measured spectra. In contrast, the ROA spectrum computed using the set of PPII structures show a sequence of $+/-$ bands in the same frequency range of 300–400 $cm^{-1}$ (Fig. 2 *A*).

Thus, the difference in the signs of the predicted ROA bands for the $\alpha_R$ and PPII conformations suggests that the ROA bands in the frequency range of 300–400 $cm^{-1}$ can be used to differentiate between the right-handed $\alpha_R$ and left-handed helical PPII conformations of Ala dipeptide (see Discussion for more detail). The Raman spectra computed using the PPII (Fig. 2 *B*) and $\alpha_R$ (Fig. 2 *D*) structures are also in good agreement with the measured spectrum. Fig. 2, *B*

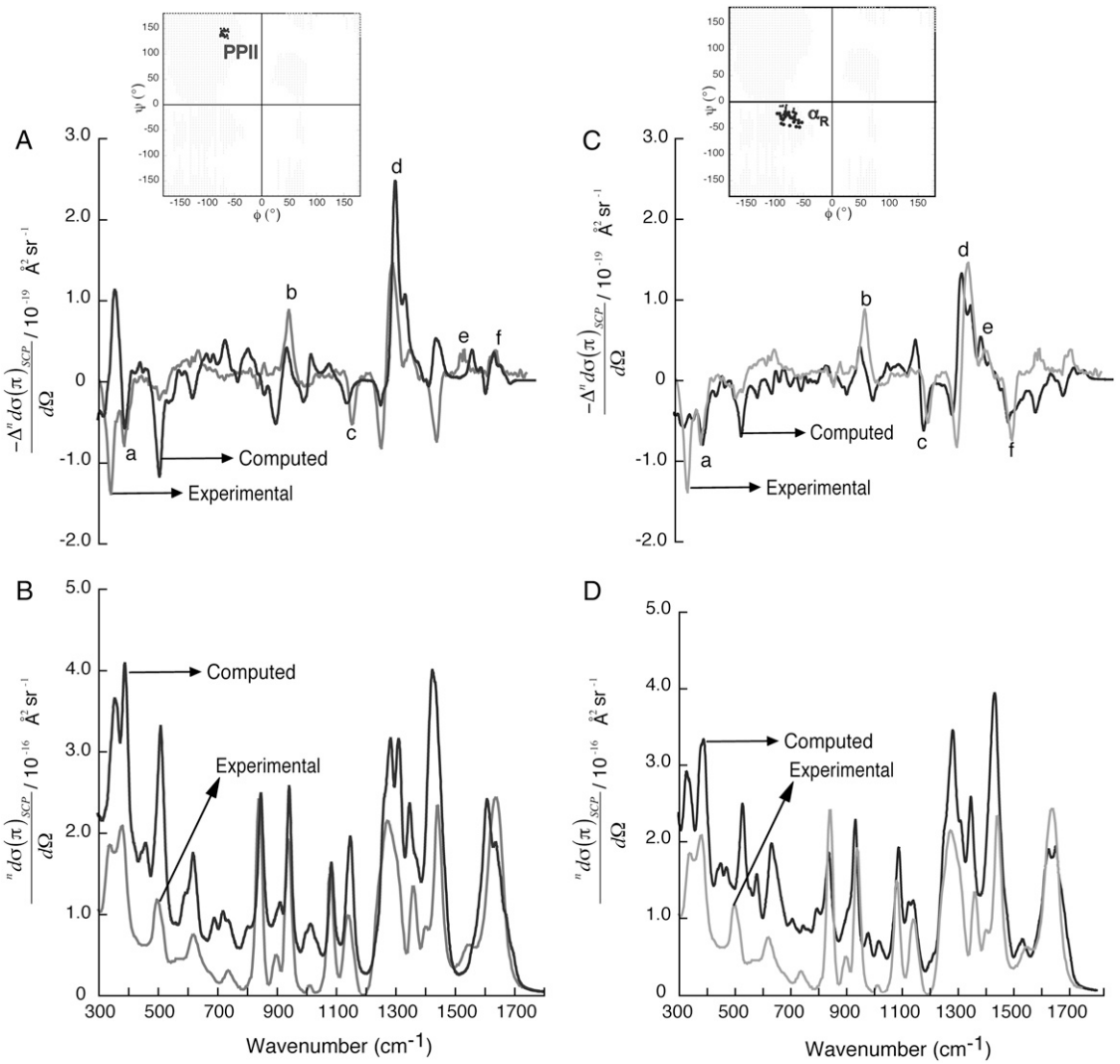


FIGURE 2 SCP backscattering ROA (*A* and *C*) and Raman (*B* and *D*) spectra of $H_2O$-Ala dipeptide clusters. The computed spectra (*black*) are averaged over a collection of dipeptide conformations from PPII (*A* and *B*) and $\alpha_R$ (*C* and *D*) regions of the Ramachandran map (*inset* in *A* and *C*). The experimental spectra (*gray*; in arbitrary units) are from Deng et al. (48).

and *D*, shows only subtle differences in the computed Raman spectra using the PPII and $\alpha_R$-conformations. For example, Raman bands at ~1140 $cm^{-1}$ (Fig. 2 *B*) and ~1540 $cm^{-1}$ (Fig. 2 *D*) are predicted for the PPII and $\alpha_R$-conformations, respectively. Thus, ROA is a better probe of the secondary structure of peptides in aqueous solution than Raman scattering experiments. A more detailed analysis of the dependence of the computed ROA spectra on the $\phi$ and $\psi$ dihedral angles of Ala dipeptide in $H_2O$ appears in the Supplementary Material (Data S1) (Section 2).

Fig. 3 shows the computed ROA (*A* and *C*) and the Raman (*B* and *D*) spectra using $D_2O$-Ala dipeptide clusters. The computed ROA spectra using both the PPII and $\alpha_R$-conformations (*insets* in Fig. 3, *A* and *C*) contain spectral features found in the measured spectrum in $D_2O$. For example, ROA bands (*peaks a–h* in Fig. 3 *A*) at 340 $cm^{-1}$ (*a*), 395 $cm^{-1}$ (*b*), 500 $cm^{-1}$ (*c*), 950 $cm^{-1}$ (*d*), 1050 $cm^{-1}$ (*e*), 1280 $cm^{-1}$ (*f*, extended amide III), 1440 $cm^{-1}$ (*g*), and 1650 $cm^{-1}$ (*h*, amide I), are predicted in the computed spectrum using the set of PPII conformations. Similarly, ROA bands (*peaks a–e* in Fig. 3 *C*) at 340 $cm^{-1}$ (*a*), 395 $cm^{-1}$ (*b*), 500 $cm^{-1}$ (*c*), 1150 $cm^{-1}$ (*d*), and 1440 $cm^{-1}$ (*e*) are predicted in the computed spectrum using the set of $\alpha_R$-conformations. Interestingly, the measured ROA spectrum of Ala dipeptide in $D_2O$ also shows a sequence of +/−/− bands in the frequency range of 300–400 $cm^{-1}$. In contrast, the measured ROA spectrum in $H_2O$ (Fig. 2) show a sequence of −/− bands between 300 $cm^{-1}$ and 400 $cm^{-1}$.

Thus, the ROA spectrum of Ala dipeptide in $D_2O$ has an additional positive band in the frequency range of 300–400 $cm^{-1}$. The ROA spectra computed using the set of PPII (Fig. 3 *A*) and $\alpha_R$ (Fig. 3 *C*) structures in $D_2O$ show a sequence of +/(−) and −/(−) bands in the frequency range of 300–400 $cm^{-1}$, respectively. The sign in parenthesis, (−),

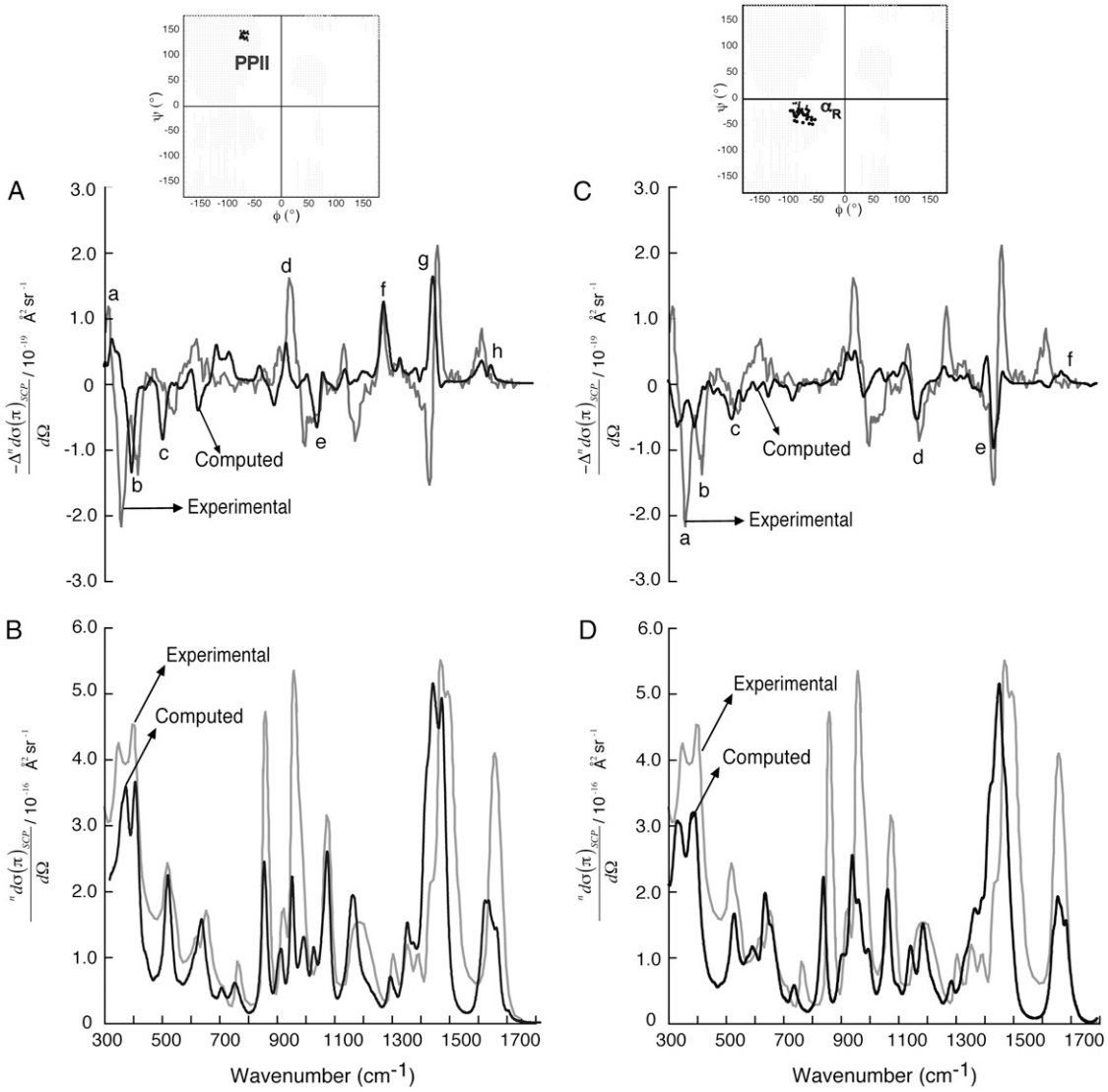


FIGURE 3 SCP backscattering ROA (*A* and *C*) and Raman (*B* and *D*) spectra of $D_2O$-Ala dipeptide clusters. The computed spectra (*black*) are averaged over a collection of dipeptide conformations from PPII (*A* and *B*) and $\alpha_R$ (*C* and *D*) regions of the Ramachandran map (*inset* in *A* and *C*). The experimental spectra (*gray*; in arbitrary units) are from Deng et al. (48).

indicates the common negative ROA band predicted in the frequency range of 300–400 $cm^{-1}$ for the PPII and $\alpha_R$-conformations. Thus, the computed ROA spectra based on PPII and $\alpha_R$ dipeptide conformations taken together contain the +/(−)/− spectral feature found in the frequency range of 300–400 $cm^{-1}$ of the measured spectrum in $D_2O$. The Raman spectra computed using the PPII (Fig. 3 *B*) and $\alpha_R$ (Fig. 3 *D*) structures are also in good agreement with the measured spectrum in $D_2O$. A more detailed analysis of the dependence of the computed ROA spectra on the $\phi$ and $\psi$ dihedral angles of Ala dipeptide in $D_2O$ appears in the Supplementary Material (Data S1) (Section 3).

There is no significant similarity between the measured and computed ROA and Raman spectra using the $\alpha_L$ (with $45° \leq \phi \leq 65°$ and $25° \leq \psi \leq 55°$) and $\beta$ (with $-180° \leq \phi \leq -125°$ and $150° \leq \psi \leq 180°$) conformations of $H_2O$-Ala dipeptide and $D_2O$-Ala dipeptide clusters (see Figs. S6 and S7 in Data S1). Thus, our ROA analysis suggests that Ala dipeptide in water populates $\alpha_R$ and PPII conformations without substantial $\alpha_L$- and $\beta$-populations.

Fig. 4 shows the relative contributions of the dipeptide, water, and peptide-water interactions to the total ROA (*A* and *C*) and Raman (*B* and *D*) scattering cross sections of Ala dipeptide-water clusters (see Eqs. 5 and 6 in Methods for more detail), computed using the PPII (*A* and *B*) and $\alpha_R$ (*C* and *D*) conformations of Ala dipeptide. The ROA and Raman scattering cross sections are influenced by water in the low frequency range of 300–1100 $cm^{-1}$ and for the amide I and II bands. However, water makes no contribution to the Raman and ROA intensities from 1200 $cm^{-1}$ to 1500 $cm^{-1}$. Kapitán

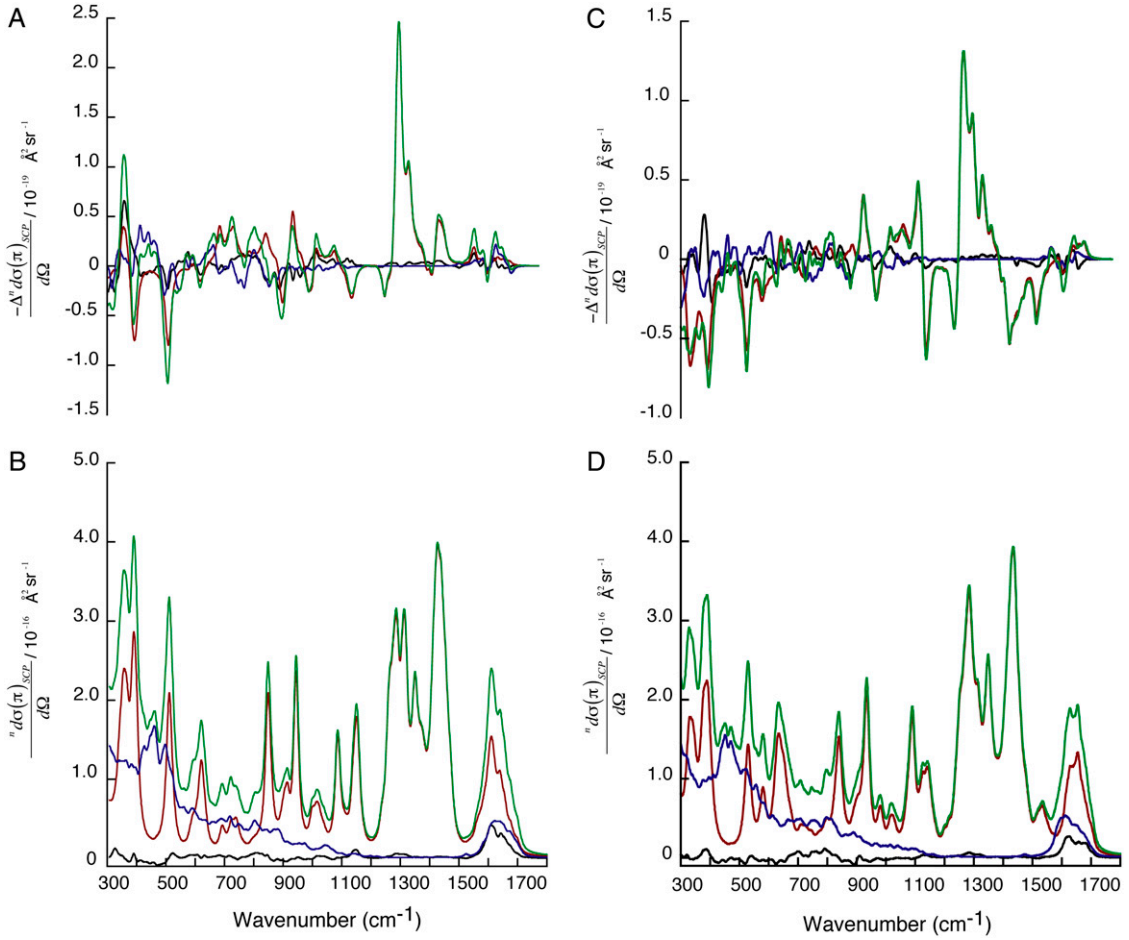


FIGURE 4 ROA (*A* and *C*) and Raman (*B* and *D*) scattering cross section contributions of Ala dipeptide (*red*), water (*blue*), and peptide-water interactions (*black*) to the total ROA and Raman scattering cross sections of Ala dipeptide-water clusters (*green*). These computed spectra are averaged over a collection of dipeptide conformations from PPII (*A* and *B*) and $\alpha_R$ (*C* and *D*) regions of the Ramachandran map.

et al. recently showed that ROA bands in the 800–1600 $cm^{-1}$ range for the proline zwitterion in aqueous solution are not influenced by water (26), consistent with our ROA analysis, which also predicts the presence of ROA bands (1200–1500 $cm^{-1}$) for Ala dipeptide in aqueous solution that are not influenced by the solvent.

Fig. 5 shows the dipeptide contributions $({}^{n}d\sigma_p, -\Delta^{n}d\sigma_p)$ of the total ROA and Raman scattering cross sections of Ala dipeptide-water cluster (see Eqs. 5 and 6 in Methods for more detail), computed using a PPII ($\phi = -68$ and $\psi = 135°$; *A* and *C*) and an $\alpha_R$ ($\phi = -73°$ and $\psi = -30°$; *B* and *D*) conformation of Ala dipeptide. The computed ROA spectra using both PPII and $\alpha_R$-conformations are in excellent agreement with the measured spectrum in both $H_2O$ (*A* and *B*) and $D_2O$ (*C* and *D*). For example, Fig. 5, *B* and *D*, shows that ROA bands *a–i* (including amides I, II, and III and the low frequency vibrational modes in the 300–400 $cm^{-1}$ range) predicted in the computed spectra using the $\alpha_R$-conformations of Ala dipeptide conformation are in excellent agreement with the measured spectra in $H_2O$ and $D_2O$.

To understand the origin of the ROA intensity differences associated with the molecular vibrations in the low frequency range (300–400 $cm^{-1}$), we decomposed those intensity differences into contributions from groups of atoms in Ala dipeptide. As proposed by Hug (58,64), the ROA intensity decompositions is illustrated using the group coupling matrices for a PPII ($\phi = -68$ and $\psi = 135°$; Fig. 6 *A*) and an $\alpha_R$ ($\phi = -73°$ and $\psi = -30°$; Fig. 6 *B*) conformation of Ala dipeptide (Fig. 6 *I*). The group coupling matrices show that the ROA intensity differences at ~364 $cm^{-1}$ (Fig. 6 *C*) for the PPII (Fig. 6 *A*) and at ~325 $cm^{-1}$ (Fig. 6 *D*) for the $\alpha_R$ (Fig. 6 *B*) are both dominated by contributions due to the relative motions of the atoms in groups 1 and 2 (Fig. 6 *I*), which is positive (*black*) and negative (*gray*) for the PPII and $\alpha_R$-conformations, respectively. Fig. 6 also shows that the ROA intensity differences associated with molecular vibrations at ~401 $cm^{-1}$ (Fig. 6 *G*) for the PPII and at ~395 $cm^{-1}$ (Fig. 6 *H*) for the $\alpha_R$ are both dominated by contributions due to the relative motions of the atoms in groups 1 and 3 (Fig. 6 *I*) and are negative for both of these conformations. Fig. 6, *E*

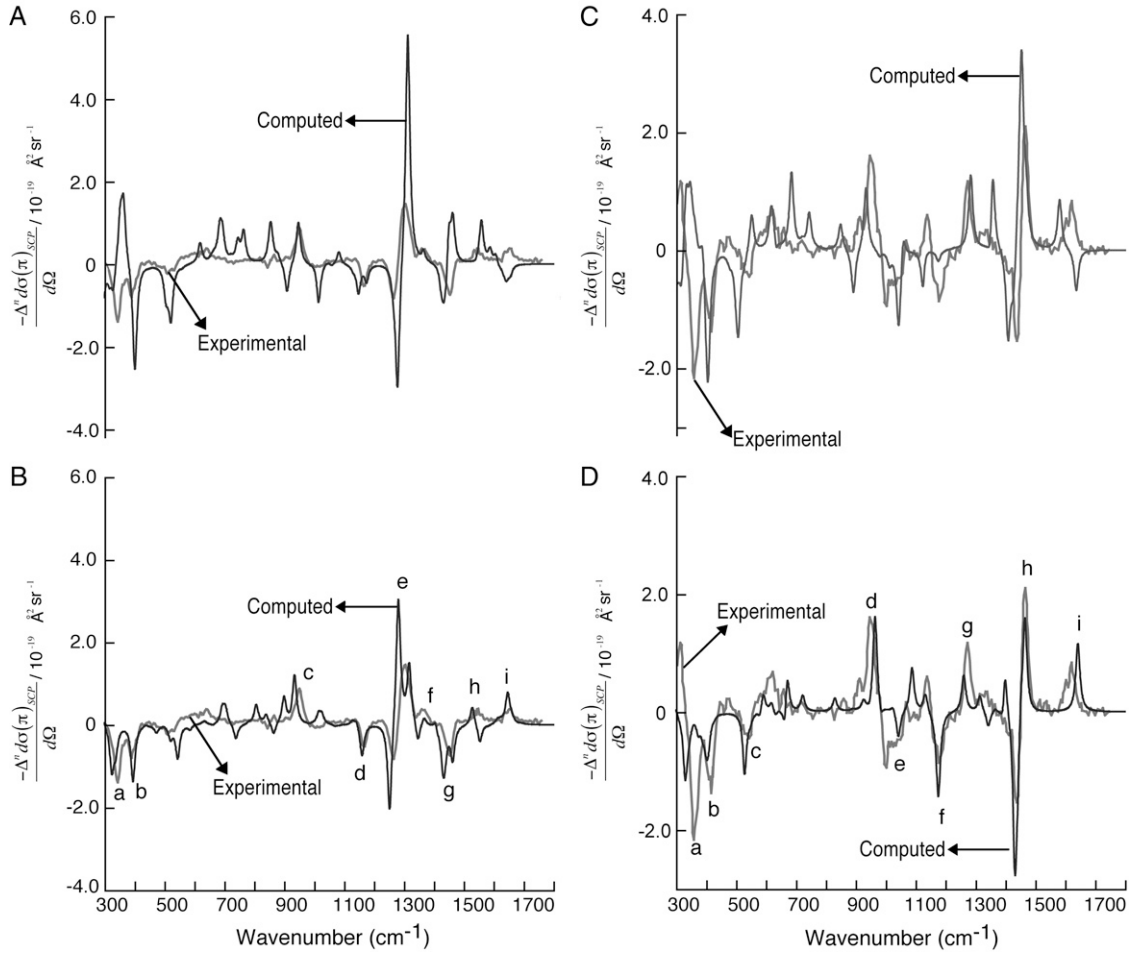


FIGURE 5 SCP backscattering ROA spectra computed (*black*) for a representative PPII ($\phi = -68°$ and $\psi = 135°$; *A* and *C*) and an $\alpha_R$-conformation of Ala dipeptide ($\phi = -73°$ and $\psi = -30°$; *B* and *D*). Experimental spectra (*gray*; in arbitrary units) in $H_2O$ (*A* and *B*) and $D_2O$ (*C* and *D*) are from Deng et al. (48).

and *F*, shows the ROA intensity differences associated with molecular vibrations at ~352 $cm^{-1}$ for the PPII conformation and at ~338 $cm^{-1}$ for the $\alpha_R$-conformation. The decomposition of the Raman intensities associated with the vibrations in these low wave number ranges for the groups of atoms in Ala dipeptide for the $\alpha_R$ and PPII conformations appear in the Supplementary Material (Data S1) (Section 5).

## DISCUSSION

The aim of this study was to characterize Ala dipeptide conformations that are consistent with the measured ROA spectra in $H_2O$ and $D_2O$. The ROA spectra were computed for $H_2O$- and $D_2O$-Ala dipeptide clusters with the PPII, $\alpha_R$-, $\alpha_L$-, and $\beta$-conformations of the dipeptide (Fig. 1 *B*) because the MC simulations found these structures in aqueous solution. Agreement between the measured and computed ROA spectra is used to characterize the populated conformations of Ala dipeptide in aqueous solution. The computed ROA spectra for the $H_2O$- and $D_2O$-Ala dipeptide clusters with the PPII and $\alpha_R$-conformations are in excellent agreement (Fig. 5) with the measured spectra. There is no significant similarity between the measured and predicted ROA spectra for the $\alpha_L$- and $\beta$-conformations. Thus, Ala dipeptide in aqueous solution dominantly populates $\alpha_R$- and PPII conformations despite the fact that $\alpha_L$- and $\beta$-structures are found in the MC simulations.

The conformational heterogeneity of Ala dipeptide has been probed using other spectroscopic methods. For example, the $^{13}$C-NMR spectra of Ala dipeptide in water and in liquid-crystalline media suggest that its structures in aqueous solution and in the liquid-crystalline state are very similar and that the structure is dominated by PPII conformations (33,34). However, these studies could not rule out the existence of $\alpha_R$ helical conformations in water. Following these NMR studies, Mehta et al. used $^{13}$C-NMR to show that Ala dipeptide in water exists in a mixture of PPII and $\alpha_R$-conformations (31), consistent with our ROA analysis. Kim et al. used 2D IR to probe the conformational heterogeneity of Ala dipeptide in aqueous solution (35). Those authors concluded

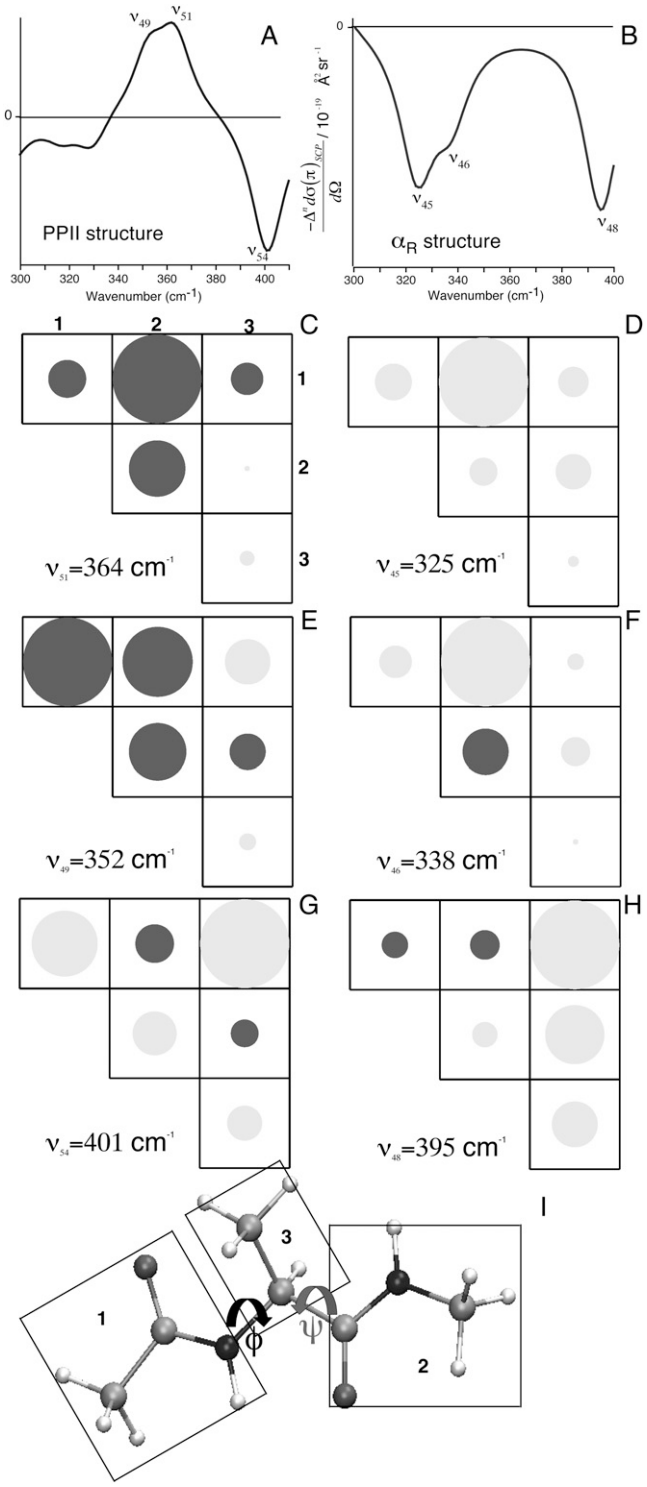


FIGURE 6 Group coupling matrices for the ROA intensity differences associated with the vibrations in the low wave number range decomposed into contributions from groups of atoms in Ala dipeptide for a PPII ($\phi = -68°$ and $\psi = 135°$; *A*) and an $\alpha_R$ ($\phi = -73°$ and $\psi = -30°$; *B*) conformation. The groups of atoms in Ala dipeptide are shown in panel *I*. Positive and negative ROA intensity differences are shown as black and gray circles, respectively.

that the 2D IR experimental data and simulations are consistent with PPII-like conformations of Ala dipeptide in aqueous solution and ruled out the possibility of $\alpha_R$ helical conformations for Ala dipeptide in water. We emphasize that the 2D IR experiments were performed in $D_2O$, which stabilizes PPII conformations compared to $H_2O$. Chellgren and Creamer have also shown that $D_2O$ stabilizes PPII conformations of alanine-containing peptides relative to $H_2O$ (65). Those authors therefore suggested that conformational analysis of peptides using NMR, vibrational circular dichroism, IR, and Raman spectroscopy of peptides in $D_2O$ is biased toward increased PPII populations.

Deng et al. suggested that the two negative ROA bands observed in the frequency range of 300–400 cm$^{-1}$ in the measured spectra of Ala dipeptide in $H_2O$ and $D_2O$ are indicative of its predominant conformation in aqueous solution (48). Our ROA computations predict the sequence of +/− and −/− ROA bands in the frequency range of 300–400 cm$^{-1}$ for the PPII and $\alpha_R$ helical conformations of Ala dipeptide, respectively (Fig. 5). Thus, the ROA analysis suggests that the two negative ROA bands observed in the frequency range of 300–400 cm$^{-1}$ in the measured spectra in $H_2O$ and $D_2O$ are characteristic of $\alpha_R$ helical conformations of Ala dipeptide. The measured ROA spectrum of Ala dipeptide in $D_2O$ (Fig. 5, *C* and *D*) also shows a positive ROA band at ~320 cm$^{-1}$ in addition to the two negative peaks in the frequency range of 300–400 cm$^{-1}$.

Our ROA spectrum computed using the PPII conformation of Ala dipeptide in $D_2O$ (Fig. 5 *C*) predicts a positive ROA band in the frequency range of 300–400 cm$^{-1}$, consistent with the measured ROA spectrum in $D_2O$. Thus, the positive ROA band in the frequency range of 300–400 cm$^{-1}$ is a characteristic of the PPII conformations of Ala dipeptide. Since $D_2O$ stabilizes PPII conformations of peptides relative to $H_2O$ (see discussion in preceding paragraph), the positive ROA band observed in $D_2O$, is not observed in the measured spectrum in $H_2O$. The predicted ROA spectra using PPII and $\alpha_R$ helical conformations of Ala dipeptide have common spectral features found in the measured spectrum in $H_2O$, which indicate that Ala dipeptide in aqueous solution displays both conformations. We emphasize that the differential ROA response of Ala dipeptide in $H_2O$ and $D_2O$—such as the key experimental spectral feature of −/− and +/−/− bands in the frequency range of 300–400 cm$^{-1}$ in $H_2O$ and $D_2O$, respectively, predicted by our calculations—demonstrates that ROA can also differentiate the PPII- and $\alpha_R$-dominant populated structures of Ala dipeptide in aqueous solution.

Han et al. also computed the ROA spectra of Ala dipeptide in $H_2O$, and their theoretical analysis of the ROA spectra suggests that PPII is the dominant conformation in aqueous solution (46). In contrast, our theoretical analysis of the ROA spectra of Ala dipeptide suggests that $\alpha_R$ is the dominant conformations in $H_2O$. If PPII dominated the conformational ensemble of Ala dipeptide in $H_2O$, then a positive ROA band

in the frequency range of 300–400 $cm^{-1}$ would characterize it (see discussion in preceding paragraph). However, the measured ROA spectrum in $H_2O$ (Fig. 5 *B*) shows two negative bands in that frequency range. The simulated ROA spectrum based on the $H_2O$-Ala dipeptide cluster with the $\alpha_R$-conformation of the dipeptide (Fig. 5 *B*) shows negative ROA bands between 300 $cm^{-1}$ and 400 $cm^{-1}$, in agreement with the measured spectrum. Thus, our ROA calculations suggest a dominant population of $\alpha_R$-conformation of Ala dipeptide in $H_2O$, which is also consistent with $^{13}C$-NMR studies (31).

Similarities between the observed and computed spectra (Figs. 2, 3, and 5) using the PPII and $\alpha_R$-conformations of Ala dipeptide suggest that the pattern of +/− and −/− ROA bands in the frequency range of 300–400 $cm^{-1}$ are characteristic of the PPII and $\alpha_R$ helical conformations for Ala dipeptide, respectively. To correlate these spectral features to molecular structural elements, we decomposed the ROA intensity differences associated with vibrations in the frequency range of 300–400 $cm^{-1}$ into contributions from nuclei in groups of atoms in Ala dipeptide for an $\alpha_R$ and a PPII conformation. For example, the ROA band at ~364 $cm^{-1}$ (Fig. 6 *A*) and ~325 $cm^{-1}$ (Fig. 6 *B*) for the PPII and $\alpha_R$, respectively, both originate from the relative motions of the nuclei in groups 1 and 2 (Fig. 6 *I*). ROA bands that are dominated by the relative motions of the nuclei in groups 1 and 2 in Ala dipeptide (Fig. 6 *I*) are also the probe of its secondary structure, since both of these groups contain the planar amide bonds that determine the $\phi$ and $\psi$ dihedral angles. Thus, the ROA spectral features in the low frequency range of 300–400 $cm^{-1}$ provide structural information of the predominant conformations of Ala dipeptide in aqueous solution.

The ROA solvent dependence for chiral molecules was computed recently using DFT. Pecul et al. used DFT combined with a continuum solvent description to examine the influence of solvent on the ROA spectra of rigid molecules (29). The authors concluded that the solvent influence on the molecular geometry, the molecular Hessian, and the optical tensors should be included when computing solvent effects on ROA. Our computation of the geometry optimization, vibrational frequencies, normal modes, and derivatives of electric dipole-electric dipole polarizability and electric dipole-magnetic dipole polarizability tensors (Eq. 4 in Methods) were carried out using Ala dipeptide-water cluster structures. Thus, including explicit water in our ROA calculations accounts for the necessary solvent effects. We also find that the ROA and Raman scattering cross sections in the low frequency range of 300–1100 $cm^{-1}$ and for the amide I and II bands are influenced by water. In contrast, the ROA and Raman bands in the frequency range of 1200–1500 $cm^{-1}$ are not affected by water (Fig. 4).

The ROA and Raman scattering cross sections arising from the peptide-water interactions (see Eqs. 5 and 6 in Methods) are a minor fraction of the total ROA and Raman scattering cross sections of an Ala dipeptide-water cluster (Fig. 4). Fig. 4 also shows that the peptide-water hydrogen-bond interactions contribute to the Raman scattering cross section of the amide I band (Figs. 4, *B* and *D*). ROA computation of polypeptide including explicit solute-solvent interactions becomes extremely time consuming as the number of atoms grows. Efficient ROA computations of polypeptides may be achieved by excluding the water contribution to the Cartesian gradients of the electric dipole-electric dipole polarizability and electric dipole-magnetic dipole polarizability. However, the solvent influence on the geometry optimization of the solute and on the molecular Hessian must be included for accurate prediction of the ROA in solution.

The accurate prediction of ROA spectra of peptides in aqueous solution requires averaging over both solvent positions and peptide geometries (66). Thus, the computed ROA spectra (Figs. 2 and 3) averaged over $H_2O$- and $D_2O$-Ala dipeptide geometries predicts ROA spectral features of Ala dipeptide in aqueous solution. Fig. 5, *B* and *D*, shows that the ROA spectra computed using a single peptide conformation with $\phi = -73°$ and $\psi = -30°$ correlates better with the observed spectrum than the computed spectrum averaged over a collection of Ala dipeptide structures with a wide range of $\phi$- and $\psi$-values ($-50° \le \phi \le -100°$ and $-50° \le \psi \le 0°$; Figs. 2 *C* and 3 *C*) from the $\alpha_R$-conformational region of the Ramachandran map. This suggests that the set of $\alpha_R$-conformations of Ala dipeptide in aqueous solution constitutes a narrow distribution of peptide geometries around $\phi = -73°$ and $\psi = -30°$, rather than the broader distribution of structures with $-50° \le \phi \le -100°$ and $-50° \le \psi \le 0°$.

Our calculations show that the predicted ROA spectra using both the PPII and $\alpha_R$-conformations of Ala dipeptide in $H_2O$ and $D_2O$ are in very good agreement with the measured spectra (Fig. 5) based on the overlap between the measured and computed spectra. Herrmann et al. recently showed that the ROA of helical peptides are dominated by the chirality associated with the peptide backbone conformation (30,67). Thus, based on the good agreement between the measured and computed spectra (Figs. 2–5) using the helical PPII and $\alpha_R$-conformations of Ala dipeptide, we suggest that the backbone conformation of Ala dipeptide in aqueous solution is characterized by the compact $\alpha_R$ and extended PPII conformations, both of which dominate in aqueous solution.

Conformational analysis of Ala dipeptide is of fundamental importance to the question of the local conformational preference of unfolded polypeptides. Our ROA computational method could be used to interpret the ROA spectra of longer unfolded polypeptides in aqueous solution and to characterize their solution conformations. To characterize conformations of unfolded polypeptides, one has to determine residue-specific Ramachandran maps of the polypeptides. We demonstrate that ROA probes of molecular chirality can be used to determine the Ramachandran map of the shortest alanine-containing peptide. The accurate description of the conformational heterogeneity of Ala dipep-

tide backbone is an important step toward defining the residue-specific conformational preferences in unfolded polypeptides. In addition to the biological significance of dipeptide conformational analysis, combined experiments and simulations on short peptides can be used to determine the accuracy of commonly used force fields in MD and MC simulations.

For example, our MC and ROA studies of Ala dipeptide show that the shortest alanine-containing peptide exists as a mixture of PPII and $\alpha_R$-conformations in aqueous solution, without a substantial population of left-handed $\alpha_L$- or $\beta$-structures, despite sampling $\alpha_L$- and $\beta$-structures in force field based MC simulations. Best et al. recently studied polyalanine peptide $A_5$ conformations in aqueous solution using MD simulations to address the question of whether the commonly used force fields overpopulate the $\alpha$-helical conformations of polyalanine peptides (10). They concluded that the NMR data are consistent with force fields that produce $\alpha$-helical populations of polyalanine peptides and that the data do not require exclusive formation of the PPII structure, consistent with our conformational analysis of Ala dipeptide in aqueous solution.

Growing access to commercial ROA spectrometers (68) and improved efficiency of ROA calculations, such as implementation of analytical derivative procedures for the computation of ROA (69), are likely to motivate further ROA analysis of aqueous polypeptide solutions. A combined conformational analysis and ROA study of polypeptides should be helpful for understanding more fully the relationship between peptide conformations and ROA spectra. A link of this kind may provide further insights into the connection between structure and dynamics.

## CONCLUSIONS

SCP ROA analysis for Ala dipeptide based on TD-DFT/DFT calculations and MC-sampled peptide-water clusters were used with experimental ROA and Raman data to assign the dominant conformations of Ala dipeptide in aqueous solution. Agreement of observed and simulated ROA spectral features indicate the viability of screening plausible MC structures based on ROA data. We find that the computed ROA spectra using a single PPII conformation with $\phi = -68$ and $\psi = 135°$ and a single $\alpha_R$-conformation with $\phi = -73°$ and $\psi = -30°$ are in excellent agreement with the observed spectra. Thus, our ROA analysis shows that Ala dipeptide adopts both $\alpha_R$ and PPII conformations in aqueous solution, which are the dominant conformations in aqueous solution.

We also find that including explicit solute-solvent interactions is required for a), adequate quantum mechanical geometry optimization of the solute conformations in solution, b), computation of the molecular Hessian, and c), computation of the solvent influence on the optical tensor for predicting the ROA spectra of peptides in solution. The accurate prediction of the ROA spectra of Ala dipeptide based on the agreement between the observed and computed spectra using the PPII and $\alpha_R$-conformations of the dipeptide in $H_2O$ and $D_2O$ suggest that our ROA computational method could be used to interpret measured ROA spectra of longer polypeptides in aqueous solution and to characterize their solution conformations.

## SUPPLEMENTARY MATERIAL

To view all of the supplemental files associated with this article, visit www.biophysj.org.

P.M. thanks Prof. Terrence G. Oas, Prof. David C. Richardson, and Prof. Jane S. Richardson for insightful discussions.

We thank the National Science Foundation (CHE-0718043) for support of this research.

## REFERENCES

1. Chen, K., Z. Liu, C. Zhou, W. C. Bracken, and N. R. Kallenbach. 2007. Spin relaxation enhancement confirms dominance of extended conformations in short alanine peptides. *Angew. Chem. Int. Ed.* 46: 9036–9039.
2. Shi, Z. S., K. Chen, Z. G. Liu, and N. R. Kallenbach. 2006. Conformation of the backbone in unfolded proteins. *Chem. Rev.* 106: 1877–1897.
3. Schweitzer-Stenner, R., and T. J. Measey. 2007. The alanine-rich XAO peptide adopts a heterogeneous population, including turn-like and polyproline II conformations. *Proc. Natl. Acad. Sci. USA.* 104:6649–6654.
4. Makowska, J., S. Rodziewicz-Motowidlo, K. Baginska, M. Makowski, J. A. Vila, A. Liwo, L. Chmurzynski, and H. A. Scheraga. 2007. Further evidence for the absence of polyproline II stretch in the XAO peptide. *Biophys. J.* 92:2904–2917.
5. Makowska, J., S. Rodziewicz-Motowidlo, K. Baginska, J. A. Vila, A. Liwo, L. Chmurzynski, and H. A. Scheraga. 2006. Polyproline II conformation is one of many local conformational states and is not an overall conformation of unfolded peptides and proteins. *Proc. Natl. Acad. Sci. USA.* 103:1744–1749.
6. Schweitzer-Stenner, R., T. Measey, L. Kakalis, F. Jordan, S. Pizzanelli, C. Forte, and K. Griebenow. 2007. Conformations of alanine-based peptides in water probed by FTIR, Raman, vibrational circular dichroism, electronic circular dichroism, and NMR spectroscopy. *Biochemistry.* 46:1587–1596.
7. McColl, I. H., E. W. Blanch, L. Hecht, N. R. Kallenbach, and L. D. Barron. 2004. Vibrational Raman optical activity characterization of poly(L-proline) II helix in alanine oligopeptides. *J. Am. Chem. Soc.* 126:5076–5077.
8. Gnanakaran, S., and A. E. Garcia. 2003. Validation of an all-atom protein force field: from dipeptides to larger peptides. *J. Phys. Chem. B.* 107:12555–12557.
9. Graf, J., P. H. Nguyen, G. Stock, and H. Schwalbe. 2007. Structure and dynamics of the homologous series of alanine peptides: a joint molecular dynamics/NMR study. *J. Am. Chem. Soc.* 129:1179–1189.
10. Best, R. B., N. V. Buchete, and G. Hummer. 2008. Are current molecular dynamics force fields too helical? *Biophys. J.* 95:L7–L9.
11. Kondru, R. K., P. Wipf, and D. N. Beratan. 1999. Structural and conformational dependence of optical rotation angles. *J. Phys. Chem. A.* 103:6603–6611.
12. Mukhopadhyay, P., G. Zuber, M. R. Goldsmith, P. Wipf, and D. N. Beratan. 2006. Solvent effect on optical rotation: a case study of methyloxirane in water. *ChemPhysChem.* 7:2483–2486.

13. Mukhopadhyay, P., G. Zuber, P. Wipf, and D. N. Beratan. 2007. Contribution of a solute's chiral solvent imprint to optical rotation. *Angew. Chem. Int. Ed.* 46:6450–6452.

14. Barron, L. D., E. W. Blanch, and L. Hecht. 2002. Unfolded proteins studied by Raman optical activity. *Adv. Protein Chem.* 62:51–90.

15. Zhu, F., J. Kapitan, G. E. Tranter, P. D. A. Pudney, N. W. Isaacs, L. Hecht, and L. D. Barron. 2008. Residual structure in disordered peptides and unfolded proteins from multivariate analysis and ab initio simulation of Raman optical activity data. *Proteins.* 70:823–833.

16. Barron, L. D., L. Hecht, and G. Wilson. 1997. The lubricant of life: a proposal that solvent water promotes extremely fast conformational fluctuations in mobile heteropolypeptide structure. *Biochemistry.* 36:13143–13147.

17. Barron, L. D. 2004. Molecular Light Scattering and Raman Optical Activity. Cambridge University Press, Cambridge, UK.

18. Nafie, L. A. 1997. Infrared and Raman vibrational optical activity: theoretical and experimental aspects. *Annu. Rev. Phys. Chem.* 48:357–386.

19. Pecul, M., and K. Ruud. 2005. Ab initio calculation of vibrational Raman optical activity. *Int. J. Quantum Chem.* 104:816–829.

20. Reiher, M., V. Liegeois, and K. Ruud. 2005. Basis set and density functional dependence of vibrational Raman optical activity calculations. *J. Phys. Chem. A.* 109:7567–7574.

21. Grimme, S., F. Furche, and R. Ahlrichs. 2002. An improved method for density functional calculations of the frequency-dependent optical rotation. *Chem. Phys. Lett.* 361:321–328.

22. Zuber, G., M. R. Goldsmith, D. N. Beratan, and P. Wipf. 2005. Towards Raman optical activity calculations of large molecules. *ChemPhysChem.* 6:595–597.

23. Zuber, G., and W. Hug. 2004. Rarefied basis sets for the calculation of optical tensors. 1. The importance of gradients on hydrogen atoms for the Raman scattering tensor. *J. Phys. Chem. A.* 108:2108–2118.

24. Haesler, J., I. Schindelholz, E. Riguet, C. G. Bochet, and W. Hug. 2007. Absolute configuration of chirally deuterated neopentane. *Nature.* 446:526–529.

25. Kapitan, J., V. Baumruk, and P. Bour. 2006. Demonstration of the ring conformation in polyproline by the Raman optical activity. *J. Am. Chem. Soc.* 128:2438–2443.

26. Kapitan, J., V. Baumruk, V. Kopecky, and P. Bour. 2006. Conformational flexibility of L-alanine zwitterion determines shapes of Raman and Raman optical activity spectral bands. *J. Phys. Chem. A.* 110: 4689–4696.

27. Liegeois, V., O. Quinet, and B. Champagne. 2005. Vibrational Raman optical activity as a mean for revealing the helicity of oligosilanes: a quantum chemical investigation. *J. Chem. Phys.* 122:214304.

28. Liegeois, V., O. Quinet, and B. Champagne. 2006. Investigation of polyethylene helical conformations: theoretical study by vibrational Raman optical activity. *Int. J. Quantum Chem.* 106:3097–3107.

29. Pecul, M., E. Larnparska, C. Cappelli, L. Frediani, and K. Ruud. 2006. Solvent effects on Raman optical activity spectra calculated using the polarizable continuum model. *J. Phys. Chem. A.* 110:2807–2815.

30. Herrmann, C., K. Ruud, and M. Reiher. 2006. Can Raman optical activity separate axial from local chirality? A theoretical study of helical deca-alanine. *ChemPhysChem.* 7:2189–2196.

31. Mehta, M. A., E. A. Fry, M. T. Eddy, M. T. Dedeo, A. E. Anagnost, and J. R. Long. 2004. Structure of the alanine dipeptide in condensed phases determined by C-13 NMR. *J. Phys. Chem. B.* 108:2777–2780.

32. Madison, V., and K. D. Kopple. 1980. Solvent-dependent conformational distributions of some dipeptides. *J. Am. Chem. Soc.* 102:4855–4863.

33. Weise, C. F., and J. C. Weisshaar. 2003. Conformational analysis of alanine dipeptide from dipolar couplings in a water-based liquid crystal. *J. Phys. Chem. A.* 107:3265–3277.

34. Poon, C. D., E. T. Samulski, C. F. Weise, and J. C. Weisshaar. 2000. Do bridging water molecules dictate the structure of a model dipeptide in aqueous solution? *J. Am. Chem. Soc.* 122:5642–5643.

35. Kim, Y. S., J. P. Wang, and R. M. Hochstrasser. 2005. Two-dimensional infrared spectroscopy of the alanine dipeptide in aqueous solution. *J. Phys. Chem. B.* 109:7511–7521.

36. Takekiyo, T., T. Imai, M. Kato, and Y. Taniguchi. 2004. Temperature and pressure effects on conformational equilibria of alanine dipeptide in aqueous solution. *Biopolymers.* 73:283–290.

37. Tran, H. T., X. L. Wang, and R. V. Pappu. 2005. Reconciling observations of sequence-specific conformational propensities with the generic polymeric behavior of denatured proteins. *Biochemistry.* 44:11369–11380.

38. Drozdov, A. N., A. Grossfield, and R. V. Pappu. 2004. Role of solvent in determining conformational preferences of alanine dipeptide in water. *J. Am. Chem. Soc.* 126:2574–2581.

39. Gnanakaran, S., and R. M. Hochstrasser. 2001. Conformational preferences and vibrational frequency distributions of short peptides in relation to multidimensional infrared spectroscopy. *J. Am. Chem. Soc.* 123:12886–12898.

40. Marsili, S., A. Barducci, R. Chelli, P. Procacci, and V. Schettino. 2006. Self-healing umbrella sampling: a non-equilibrium approach for quantitative free energy calculations. *J. Phys. Chem. B.* 110:14011–14013.

41. Laio, A., and M. Parrinello. 2002. Escaping free-energy minima. *Proc. Natl. Acad. Sci. USA.* 99:12562–12566.

42. Smith, P. E. 1999. The alanine dipeptide free energy surface in solution. *J. Chem. Phys.* 111:5568–5579.

43. Ensing, B., M. De Vivo, Z. W. Liu, P. Moore, and M. L. Klein. 2006. Metadynamics as a tool for exploring free energy landscapes of chemical reactions. *Acc. Chem. Res.* 39:73–81.

44. Rosso, L., J. B. Abrams, and M. E. Tuckerman. 2005. Mapping the backbone dihedral free-energy surfaces in small peptides in solution using adiabatic free-energy dynamics. *J. Phys. Chem. A.* 109:4162–4167.

45. Duan, Y., C. Wu, S. Chowdhury, M. C. Lee, G. M. Xiong, W. Zhang, R. Yang, P. Cieplak, R. Luo, T. Lee, J. Caldwell, J. M. Wang, and P. Kollman. 2003. A point-charge force field for molecular mechanics simulations of proteins based on condensed-phase quantum mechanical calculations. *J. Comput. Chem.* 24:1999–2012.

46. Han, W. G., K. J. Jalkanen, M. Elstner, and S. Suhai. 1998. Theoretical study of aqueous *N*-acetyl-L-alanine *N′*-methylamide: structures and Raman, VCD, and ROA spectra. *J. Phys. Chem. B.* 102:2587–2602.

47. Jalkanen, K. J., I. M. Degtyarenko, R. M. Nieminen, X. Cao, L. A. Nafie, F. Zhu, and L. D. Barron. 2008. Role of hydration in determining the structure and vibrational spectra of L-alanine and *N*-acetyl L-alanine *N′*-methylamide in aqueous solution: a combined theoretical and experimental approach. *Theor. Chem. Acc.* 119:191–210.

48. Deng, Z., P. L. Polavarapu, S. J. Ford, L. Hecht, L. D. Barron, C. S. Ewig, and K. Jalkanen. 1996. Solution-phase conformations of *N*-acetyl-*N′*-methyl-L-alaninamide from vibrational Raman optical activity. *J. Phys. Chem.* 100:2025–2034.

49. Jorgensen, W. L., D. S. Maxwell, and J. TiradoRives. 1996. Development and testing of the OPLS all-atom force field on conformational energetics and properties of organic liquids. *J. Am. Chem. Soc.* 118:11225–11236.

50. Jorgensen, W. L., J. Chandrasekhar, J. D. Madura, R. W. Impey, and M. L. Klein. 1983. Comparison of simple potential functions for simulating liquid water. *J. Chem. Phys.* 79:926–935.

51. Jorgensen, W. L., and J. Tirado-Rives. 2005. Molecular modeling of organic and biomolecular systems using BOSS and MCPRO. *J. Comput. Chem.* 26:1689–1700.

52. Allen, M. P., and D. J. Tildesley. 1987. Computer Simulations of Liquids. Oxford University Press, Oxford, UK.

53. Dewar, M. J. S., E. G. Zoebisch, E. F. Healy, and J. J. P. Stewart. 1985. The development and use of quantum-mechanical molecular-models. 76. Am1—a new general-purpose quantum-mechanical molecular-model. *J. Am. Chem. Soc.* 107:3902–3909.

54. Storer, J. W., D. J. Giesen, C. J. Cramer, and D. G. Truhlar. 1995. Class-IV charge models—a new semiempirical approach in quantum-chemistry. *J. Comput. Aided Mol. Des.* 9:87–110.

55. Luber, S., C. Herrmann, and M. Reiher. 2008. Relevance of the electric-dipole-electric-quadrupole contribution to Raman optical activity spectra. *J. Phys. Chem. B*. 112:2218–2232.

56. Barron, L. D., and A. D. Buckingham. 1971. Rayleigh and Raman scattering from optically active molecules. *Mol. Phys.* 20:1111–1119.

57. Barron, L. D., and J. R. Escribano. 1985. Stokes-antistokes asymmetry in natural Raman optical-activity. *Chem. Phys.* 98:437–446.

58. Hug, W. 2001. Visualizing Raman and Raman optical activity generation in polyatomic molecules. *Chem. Phys. Lett.* 264:53–69.

59. Ahlrichs, R., M. Bär, H.-P. Baron, R. Bauernschmitt, S. Böcker, M. Ehrig, K. Eichkorn, S. Elliott, F. Furche, and F. E. A. Haase. 2002. TURBOMOLE 5.6.

60. Eichkorn, K., F. Weigend, O. Treutler, and R. Ahlrichs. 1997. Auxiliary basis sets for main row atoms and transition metals and their use to approximate Coulomb potentials. *Theor. Chem. Acc.* 97:119–124.

61. Lovell, S. C., I. W. Davis, W. B. Adrendall, P. I. W. de Bakker, J. M. Word, M. G. Prisant, J. S. Richardson, and D. C. Richardson. 2003. Structure validation by C $\alpha$ geometry: $\phi$,$\psi$ and C $\beta$ deviation. *Proteins Struct. Funct. Genet.* 50:437–450.

62. Zhu, F. J., N. W. Isaacs, L. Hecht, and L. D. Barron. 2005. Raman optical activity: a tool for protein structure analysis. *Structure*. 13: 1409–1419.

63. Reference deleted in proof.

64. Zuber, G., and W. Hug. 2004. Computational interpretation of vibrational optical activity: the ROA spectra of (4*S*)-4-methylisochromane and the (4*S*)-isomers of *Galaxolide*®. *Helv. Chim. Acta*. 87:2208–2234.

65. Chellgren, B. W., and T. P. Creamer. 2004. Effects of $H_2O$ and $D_2O$ on polyproline II helical structure. *J. Am. Chem. Soc.* 126:14734–14735.

66. Kapitan, J., V. Baumruk, R. Pohl, and P. Bour. 2006. Proline zwitterion dynamics in solution, glass and crystalline state. *J. Am. Chem. Soc.* 128:13451–13462.

67. Herrmann, C., K. Ruud, and M. Reiher. 2007. Importance of backbone angles versus amino acid configurations in peptide vibrational Raman optical activity spectra. *Chem. Phys.* 343:200–209.

68. BioTools. http://www.btools.com.

69. Liegeois, V., K. Ruud, and B. Champagne. 2007. An analytical derivative procedure for the calculation of vibrational Raman optical activity spectra. *J. Chem. Phys.* 127:204105.